


Effects of biochar on hydration, strength degradation, and alkali-silica reaction in sustainable waste glass sand-based mortars

Xuqun Lin^a, Tianxing Shi^{a,*}, Quang Dieu Nguyen^{a,**} , Arnaud Castel^a, Vivian W.Y. Tam^b

^a School of Civil and Environmental Engineering, University of Technology Sydney, NSW, 2007, Australia

^b Western Sydney University, School of Engineering, Design and Built Environment, NSW, 2751, Australia

ARTICLE INFO

Keywords:

Biochar
Waste glass
ASR
Microstructure
Sustainability

ABSTRACT

The biochar in concrete structures has attracted a lot of attention, offering new biomass recycling strategies while improving mechanical and durability properties of the biochar-cement composites. This study investigated the alkali-silica reaction (ASR) in waste glass sand-based mortars with three biochar, including corn cob biochar (CCB), waste wood biochar (WWB), and rice husk biochar (RHB), using the accelerated mortar bar test (AMBT) up to 96 days. Due to the fine biochar size ($<100\ \mu\text{m}$, $D_{90} = 34.67\ \mu\text{m}$), samples with 5 wt% CCB exhibited the lowest mortar bar expansion and mass gain up to 96-day of exposure in 1M NaOH bath at $80\ ^\circ\text{C}$, while experiencing the lowest strength loss. X-ray diffraction patterns indicated increased intensity of ASR gels, including tobermorite-type C-S-H and alkali-silicate-hydrates (ASH) in all groups. Thermogravimetric analysis (TG) results revealed that CCB5 had the lowest mass loss of ASR gels after 96 days in the 1M NaOH bath. Biochar degradation due to ASR was observed using Backscattered Electron images. Finally, it was recommended that up to 10 wt% fine-size corn cob biochar ($<100\ \mu\text{m}$, $D_{90} = 34.67\ \mu\text{m}$) could be conservatively used to partially replace cement content for sustainable concrete design.

1. Introduction

Concrete has been used to build numerous complex structures for decades, attributing to its durable and stable characteristics. However, as one of the most used binder materials in construction section, cement manufacturing accounts for up to 7 % of the global greenhouse gas emissions [1,2]. Miller et al. [3] reported that the cement production would be further increased in the next decades due to ageing infrastructure repair and expansion of urbanisation, raising the environmental concerns, e.g. increased CO_2 emissions. Likewise, Imbabi et al. [4] estimated that the production of cement could be quadrupled from 2012 to 2050, posing a significant challenge in the environment management in the globe. Thus, finding proper solutions to reduce cement content in concrete have emerged as an urgent matter for researchers and scientists.

Recycling industrial by-products, such as granulated blast furnace slag (GGBFS) [5,6], fly ash (FA) [7,8], paper wastes [9,10], and combination of limestone and calcined clay (LC3) [11,12] have been the most common approach to reduce the carbon footprint of sustainable concrete structures. In a study by Sun and Zhang [13], the presence of GGBFS refined the cementitious microstructure, led

* Corresponding author.

** Corresponding author.

E-mail addresses: tianxing.shi-1@student.uts.edu.au (T. Shi), quangdieu.nguyen@uts.edu.au (Q.D. Nguyen).

to a compressive strength increase by 8 % and reduced passing charges in rapid chloride penetration test (RCPT) when compared to the reference group at 360 days. Similarly, Ukpata et al. [14] found that GGBFS promoted the chloride-binding capacity of samples with GGBFS, improving the resistance against chloride ion ingress. In a chloride desorption test by Teymnouri and Shakouri et al. [15], they

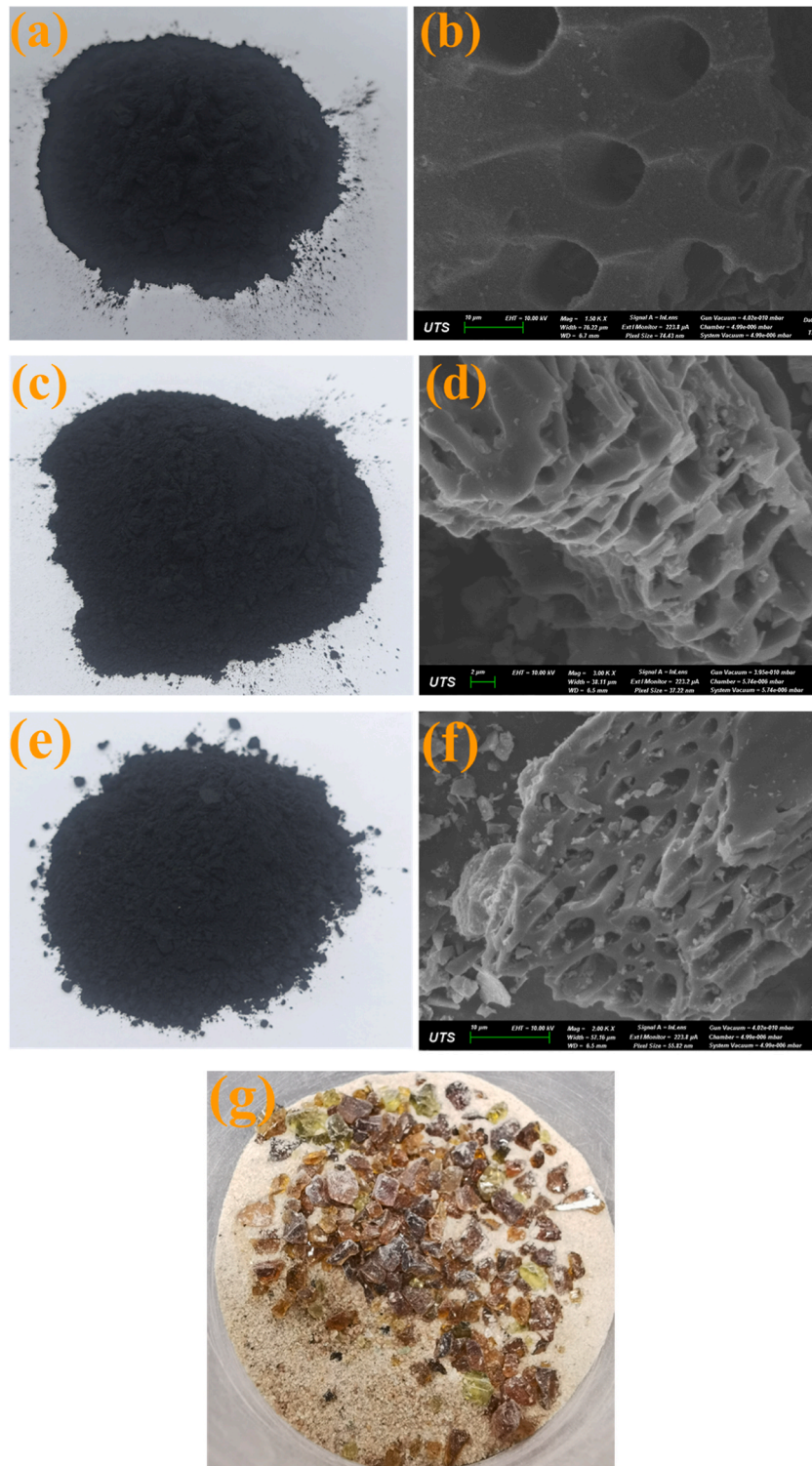


Fig. 1. Morphologies of materials: (a) Blended waste wood biochar (WWB); (b) SEM image of WWB; (c) Corn cob biochar (CCB); (d) SEM image of CCB; (e) Rice husk biochar (RHB); (f) SEM image of RHB; (g) Waste glass sand (WGS) before sieving.

reported that up to 30 wt% FA improved the chloride binding capacity of FA-cement composites when compared to FA-free samples, attributed to more formations of monocarboaluminate (Mc) in the pozzolanic reactions. Li et al. [16] observed that FA addition led to a denser microstructure comparing to the control group in a mercury intrusion porosimetry (MIP) test. Zunino et al. [17] reported that a denser microstructure was observed in LC3 samples, due to combination of filler effects of limestone and formation of Mc refining pores of the LC3-cement matrix. Although those by-products could be utilised as supplementary cementitious materials (SCMs) to partially replace cement content designing sustainable concrete, the geographical availability of these SCMs limits their applications for countries without such material supply, posing concerns regarding relatively high material transportation cost and raise of the carbon footprint. Consequently, it is necessary to find other appropriate alternatives as SCMs with local material availability.

Recently, the application of biochar as SCMs has attracted attention [18–21]. Biochar is produced from various biomass wastes subjected to the oxygen-limited pyrolysis, offering a new recycling strategy rather than conventional biomass burning or landfilling [22–25]. Gupta et al. [26] reported that using 2 wt% dry wood dusk biochar to replace cement content led to 7-day and 28-day compressive strength increase by 22.6 % and 7.7 % respectively. They observed that, due to water retention at early curing age, biochar pores offered additional hydration sites with humidity promoting the cement hydration and denser microstructure. Aziz et al. [27] used 1.5 wt% date palm leaves biochar as cement replacement, showing that biochar mortars' ultrasonic velocity and thermal conductivity were reduced by 9.5 % and 41 % respectively when compared to the reference group. Kang et al. [28] reported that, after replacing cement by 4.5 wt% coconut shell biochar, they found that the 28-day flexural strength was improved by 11 %, being attributed to filling effects of biochar. In a study by Mo et al. [29], 2 wt% weed tree biochar reduced the autogenous shrinkage of the biochar-cement composites by 16.3 % and improved the relative humidity by 4.5 % after 180-h curing. Furthermore, several studies [30–32] showed that lower strength loss was observed for biochar-cement composites exposed to sulphate and chloride solutions, revealing improved diffusion resistance against aggressive ions. Based on aforementioned literature, the addition of biochar seems to be effective in reduce the permeability of the biochar-cement composites, having potential in mitigating the ASR expansion of the cementitious composites by limiting the access of alkali ions. In addition, Deng et al. [33] found that the addition of polyvinyl alcohol (PVA) fibres improved the cracking energy adsorption and reduced brittleness, improving the ASR expansion resistance of the PVA-cement composites. In this regard, biochar seems to share similar characteristics with PVA to physically mitigate ASR expansion of cementitious composites. However, despite that many studies have been carried out to investigate the effects of biochar in both mechanical and durability properties of the biochar-modified cementitious composites, there is a lack of understanding of how biochar may affect the alkali-silica reactions (ASR) of the biochar-cement mortars or concrete, regarding biochar type and cement replacement percentage.

This study aims to analyse the effects of various biochar on ASR resistance of the biochar-cement mortars, including corn cob biochar (CCB), rice husk biochar (RHB), and blended waste wood biochar (WWB). The hydration kinetics of samples with different biochar were compared. ASR development in samples exposed to 1M NaOH bath at 80 °C was analysed based on comparisons of mortar expansion, mass change, and strength degradation up to 96 days of exposure. Phase changes at different NaOH solution exposure periods were investigated using X-ray diffraction (XRD) and Thermogravimetric analysis (TG). Backscattered Electron imaging (BSE) together with Energy Dispersive X-ray Spectroscopy (EDS) were used to identify and analyse the chemical compositions of ASR products in samples with and without biochar.

2. Methodology

2.1. Raw materials and specimen fabrications

General purpose cement (GP) traded by Boral Australia was used to fabricate the mortar samples. Two local commercial biochar, including blended waste wood biochar (WWB) and rice husk biochar (RHB) were supplied by Rainbow Bee Eater Biochar (Australia). These two biochar were processed through pyrolysis at a temperature of 500 °C for 1 h. The third biochar corn cob biochar (CCB) was obtained from Fanernuo Biochar Company (Xuchang, China). It should be noted that CCB was produced in the same condition as WWB and RHB, mitigating the variance due to different pyrolysis methods. After drying in an oven at temperature of 80 °C for a week, the three biochar were ground for 30 s using a ring mill (Fig. 1). To improve the sustainability of biochar-cement mortars, waste glass sand (WGS) was utilised as reactive fine aggregate [34–36]. Waste glass bottles were collected from a local recycling station in Sydney, Australia. It should be noted that all waste glass bottles were carefully cleaned, and dried in an oven at a temperature of 70 °C for a week. Initially, a rubber hammer was used to break waste glass bottles into small pieces. Glass pieces were then ground into waste glass sand (WGS) using a Fritsch Jaw Crusher with a size limit of 4 mm (Fig. 1g). After that, WGS was sieved to achieve a particle size distribution as per ASTM C1260 requirements [37] (Table 1). Based on the SEM images in Fig. 1, WWB particles have thick walls with round pores (Fig. 1b), while eclipse-shape pores are randomly distributed in RHB particles (Fig. 1f). Fig. 1d presents a significantly different morphology of pores with irregular shape in CCB particles.

Fig. 2 shows the particle size distribution of the raw powders. Among the three biochar, WWB had relatively a coarser particle size

Table 1
Particle size distribution of WGS.

Sieving size (μm)	<0.3	0.3–06	0.6–1.18	1.18–2.36	2.36–4.75
Mass (%)	15	25	25	25	10

(up to 239.88 μm) with a D50 value of 19.95 μm and a D90 value of 79.43 μm . CCB had the finest particle size (up to 100 μm) with a D50 value of 13.18 μm and a D90 value of 34.67 μm , while RHB (up to 178.48 μm) had a D50 value of 13.18 μm and a D90 value of 69.18 μm . Table 2 presents the chemical compositions of all powders, and Table 3 shows the physical properties of the three biochar as given by two companies. The top three oxides in the three biochar were SiO_2 , Al_2O_3 , and CaO . The XRF results of WGS revealed that brown waste glass contained 69.75 % SiO_2 and 12.75 % Na_2O .

Table 4 demonstrates the mix design of all groups. The water-binder ratio of 0.47 was adopted. The specimen fabrication programme is shown in Table 5. CWG group is the control group as benchmark. This study adopted two replacement percentages, including 5 wt% (named as RHB5, CCB5 and CWB5) and 10 wt% biochar (named as RHB10, CCB10, and CWB10). As a result, the effects of various biochar on the mortar expansion, mass change, and strength degradation could be compared. It is worth noting that additional samples were casted and cured in a water tank at room temperature (Table 5), allowing to assess the mechanical strength degradation of the specimens exposed to the 1M NaOH bath.

Firstly, all binders were premixed using a 10L Hobar Mixer at a low speed of 16 rpm for 1.5 min s, obtaining a uniform binder mixture. Then the powder mixture was poured into a dry container. Dry WGS with different sizes (Table 2) was mixed with half water content at low-speed ration for 2 min. Another 3-min mixing at 24 rpm was set after adding the powder mixture and the rest of water content. It should be noted that Superplasticiser (Sikament® Eco WR, Sika Australia) was added to the fresh mixture with biochar, achieving similar flows when compared to the control group (Table 4). Then, the fresh mortar mixtures were poured into corresponding moulds as listed in Table 5. A 2-min vibration was performed to all moulds achieving desirable compaction. It is worth mentioning that plastic foil was used to cover all moulds till 24-h demoulding.

Sodium hydroxide pellet (Rowi Scientific, Australia) was used to prepared 1M NaOH solution. It should be noted that samples exposed to the NaOH solution bath were marked and cured in a water bath at 80 °C for 24 h as per ASTM C1260-23 [37].

2.2. Hydration kinetics

Paste samples were casted using the same mix design in Table 4 without using fine aggregate. Approximately 10 g of each fresh paste was placed in a labelled calorimeter container. The heat evolution of each group was recorded using a TAM air isothermal calorimetry. The temperature of 20 °C was set, and the hydration heat recording period was set up to 72 h.

2.3. Accelerated mortar bar test (AMBT)

AMBT samples were initially immersed in water at 80 °C for 24 h before obtaining the zero reading as per ASTM C1260-23 [37]. Then, each sample was removed from the 80 °C water tank, zero reading was measured using a comparator (precision of 1 μm) after wiping the surface solution on each sample using a towel within 5 s. After that, each sample were continuously immersed in the 1M NaOH solution bath at 80 °C until 96 days. The length of the mortar samples was the average value of three identical samples at each designated measuring time.

2.4. Mass change

After 24-h water bath at 80 °C, each sample was wiped using a towel and weighted using a digital balance to record the zero reading. Following the same curing regime as AMBT set up, the mass of all groups was measured accordingly. The mass change of each group was the average weight of three mortars at each measuring time.

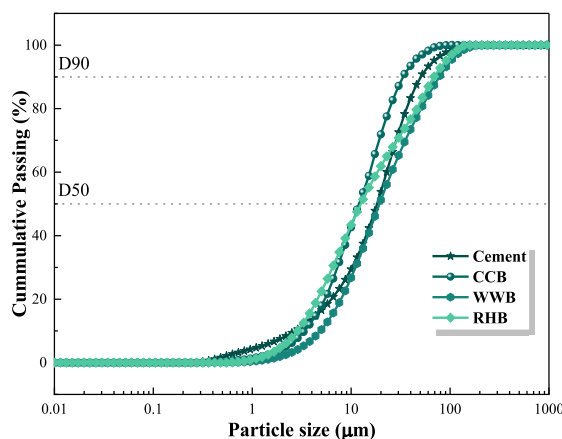


Fig. 2. Particle size distribution of powders.

Table 2
XRF results.

Chemical compositions	Cement	CCB	RHB	WWB	WGS
SiO ₂	18.94	51.97	73.99	57.62	69.75
CaO	63.73	15.48	11.91	19.15	9.72
Al ₂ O ₃	5.14	12.83	5.78	3.95	2.4
P ₂ O ₅	0.20	5.68	0.77	2.29	–
SO ₃	2.49	1.82	0.29	1.33	0.49
Na ₂ O	0.25	2.34	0.83	5.15	12.75
MgO	1.48	2.82	1.1	3.15	2.15
K ₂ O	0.47	3.44	3.83	1.58	0.81
TiO ₂	0.29	0.31	0.09	0.12	–
V ₂ O ₅	0.02	0.01	0.01	0.03	–
Fe ₂ O ₃	3.00	2.92	0.94	1.67	–
L.O.I.	3.989	0.38	0.46	3.96	1.93

Table 3
Physical properties of biochar.

Biochar type	Specific surface area (m ² /g)	Density (g/cm ³)	pH value
CCB	27.21	0.89	9.82
WWB	2.35	1.59	8.35
RHB	13.89	0.45	8.96

Table 4
Mortar mix design.

Mix designs	GPC	Water	WGS	RHB	CCB	WWB	Superplasticiser	Water/binder ratio	Flow (mm)
CWG	1	0.47	2	–	–	–	–	0.47	179 ± 2.7
RHB5	0.95	0.47	2	0.05	–	–	0.008	0.47	180 ± 1.9
RHB10	0.9	0.47	2	0.1	–	–	0.016	0.47	178 ± 2.5
CCB5	0.95	0.47	2	–	0.05	–	0.008	0.47	181 ± 2.6
CCB10	0.9	0.47	2	–	0.1	–	0.016	0.47	177 ± 3.2
CWB5	0.95	0.47	2	–	–	0.05	0.008	0.47	180 ± 2.1
CWB10	0.9	0.47	2	–	–	0.1	0.016	0.47	179 ± 3.3

Note: GPC means general purpose cement, WGS refers to waste glass sand, RHB is rice husk biochar, CCB means corn cob biochar, and WB is blended wood biochar.

Table 5
Specimens and testing programme.

Testing method	samples	Mould dimensions	Exposure condition
28-day and 96-day compressive strength	3,3	50mm × 50mm × 50mm	28-day/96-day curing in water tank @ room temperature
28-day and 96-day compressive strength	3,3	50mm × 50mm × 50mm	28-day/96-day curing in 1M NaOH bath @ 80 °C
28-day and 96-day flexural strength	3,3	40mm × 40mm × 160mm	28-day/96-day curing in water tank @ room temperature
28-day and 96-day flexural strength	3,3	40mm × 40mm × 160mm	28-day/96-day curing in 1M NaOH bath @ 80 °C
Mass change	3	40mm × 40mm × 160mm	Up to 96-day exposure in 1M NaOH bath @ 80 °C
Accelerated mortar bar test (AMBT)	3	25mm × 25mm × 285mm with steel pin attached at each end	Up to 96-day exposure in 1M NaOH bath @ 80 °C

2.5. Strength degradation

Based on Table 5, three cubes and prisms of each group were exposed to water at room temperature and 1M NaOH bath at 80 °C for 28 days and 96 days. As per ASTM C109-20 [38], 28-day and 96-day compressive strength was measured using a UH500 universal testing machine. AGX50 universal testing machine was used to test 28-day and 96-day flexural strength of samples with and without NaOH solution exposure complying with ASTM C348-21 [39]. It is worth noting that 3 samples of each group were tested for each immersion conditions, and mechanical strength degradations at 28 days and 96 days were the average of three identical testing results.

2.6. Microstructure analysis

Broken pieces obtained following the 28-day and 96-day mechanical tests were placed in a 99 % isopropanol solution for 24 h to stop the hydration process, followed by a drying process at 50 °C for 10 days. Half amount of sample pieces was ground to pass a 200- μ m sieve. The rest sample pieces for BSE analysis were casted in cylinder moulds using epoxy resin for 24 h. After that, polishing process was performed as per guidelines in literature [40]. Finally, polished samples were continuously dried in an oven with temperature of 50 °C for 7 days. A Quorum Q150V coater was utilised to perform 12 nm-chromium coating on each sample. BSE analysis was carried out using a Zeiss EVO Scanning Electron Microscopy (SEM) with energy dispersive X-ray spectroscopy (EDS). The working distance was set 9–10 mm at voltage of 15 kV.

XRD analysis was performed using a Bruker D8 Discover diffractometer ($\text{Cu K}\alpha$, $\lambda = 1.54 \text{ \AA}$). The scanning step of 0.02° from 5° to 70° 2θ was adopted. The crystalline phases in each group were analysed using Crystallography Open Database.

TG analysis at a temperature up to 1000 °C was carried out using a NETZSCH STA 449 Jupiter. The heating rate was set as $10^\circ\text{C}/\text{min}$. Approximately 30 mg of each mortar powder was stored in an alumina crucible, followed by a 10-min standby in the N_2 -environment chamber. Based on literatures [41,42], the N_2 flow was set at 50 ml/min for all TG analysis. Finally, TG and derivative TG (DTG) results were used for phase calculations for samples exposed to water and in 1M NaOH solution bath at 28 days and 96 days.

3. Results

3.1. Hydration kinetics

The effects of the different biochar at two cement replacement rates on the hydration kinetics are illustrated in Fig. 3, including normalised heat flow (Fig. 3a) and normalised heat (Fig. 3b). It should be noted that the hydration evolutions were interpreted as per gram for each mix design. As shown in Fig. 3a, an hydration peak delay of 1 h and 1.5 h were observed for samples with 5 wt% and 10 wt% biochar respectively when compared to the control group (brown line).

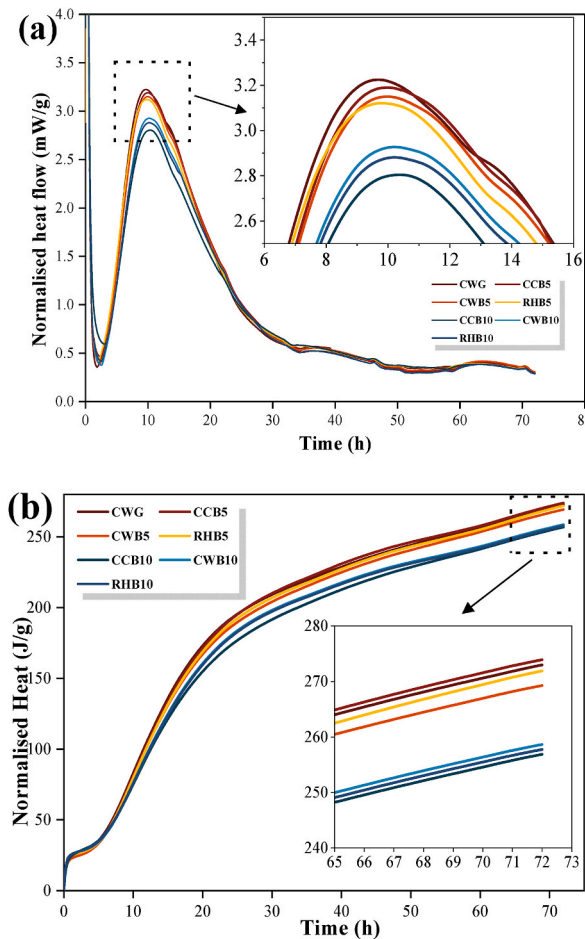


Fig. 3. Hydration kinetics of mortars with and without biochar: (a) Normalised heat flow; (b) Normalised heat.

At the major heat peak from 8 h to 11 h of hydration, CWG group exhibited the highest heat flow peak of 3.22 mW/g after 9 h of hydration. For samples with 5 wt% biochar, a comparable heat flow peak of 3.19 mW/g was observed for CCB5 group in dark-red line after 10.1 h of hydration. CWB5 group and RHB5 group showed a slight heat peak reduction of 0.06 mW/g and 0.07 mW/g respectively when compared to CWG group. As shown in Fig. 2, CCB ($<100\ \mu\text{m}$) had the finest particle size, remaining comparable heat peaks as the control group, while coarser biochar led to slight heat peak reductions. This finding was consistent with the study by Gupta et al. [43]. They reported that 5 wt% ultra-fine wood biochar ($<10\ \mu\text{m}$, $D_{90} = 9\ \mu\text{m}$) improved the heat peak by 0.25 mW/g when compared to the reference group with a water to binder ratio of 0.5:1. This phenomenon could be explained by a higher content of finer biochar particle providing more hydration sizes and improving the cement hydration when compared to plain cement pastes. In this study, the D_{90} value of CCB, CWB, and RHB is $34.67\ \mu\text{m}$, $79.43\ \mu\text{m}$, and $69.18\ \mu\text{m}$ respectively (Fig. 2). High content of coarser biochar particles seemed to negatively impact on the hydration development of the fresh cementitious mixture, e.g. 0.06–0.07 mW/g peak reduction in CWB5 and RHB5 group. This finding had a good agreement with a finding by Dixit et al. [44], reporting slight heat peak delay and reduction for samples with 5 wt% wood dust biochar ($<300\ \mu\text{m}$, $D_{90} = 200\ \mu\text{m}$). In terms of 10 wt% cement replacement, noticeable heat peak reductions of 0.3–0.45 mW/g were observed. Regardless of the biochar size, the presence of 10 wt% biochar led to a cement dilution effect, reducing the heat peak by up to 14.1 % when compared to the reference group. Similarly, Zhang et al. [45] used 10 wt% sludge-based biochar to partially replace cement, reporting that excessive biochar addition led to a heat peak reduction of 0.25 mW/g.

Fig. 3b depicts the normalised heat for all groups after 72 h of hydration. CCB5 group exhibited the highest normalised heat of 274.01 J/g. Due to relatively coarser particle ($<239.88\ \mu\text{m}$, $D_{90} = 79.43\ \mu\text{m}$), CWB5 had the lowest heat of 269.2 J/g among the three biochar, having a comparable heat release than that of the control group (271.5 J/g). However, up to 8 % heat reduction was observed for samples with 10 wt% biochar, highlighting the negative effects on the hydration development of biochar-cement composites due to the cement dilution effect.

3.2. Mortar expansion analysis

The ASR kinetics and expansion results for all groups are presented in Fig. 4. Each expansion value is the average result of three identical samples. The results revealed different mitigation performances related the cement replacement ratios. Samples with 5 wt% biochar displayed slight reductions in the 28-day and 96-day mortar expansions by 4.2–7.2 % and 3.7–6.87 % respectively when compared to that of the reference group. Samples with 10 wt% biochar exhibited slightly higher expansion when compared to the CWG group at all measuring times, being 5.7–12.1 % and 7.2–9.4 % for 28-day and 96-day mortar expansion respectively. By contrast, Biochar seem not as effective as other SCMs, such as GGBFS [46,47] or FA [48,49] in mitigating ASR expansion.

The poor ASR migration performances may be governed by two aspects: firstly, it should be noted that due to the porous nature of the biochar particles (Fig. 1), more accessible channels were formed for Na^+ and water to penetrate into the cementitious matrix. Higher biochar content (e.g. 10 wt%) would inevitably lead to a more porous cementitious matrix than samples with low biochar content [22,30,48]. Secondly, these three biochar did not offer sufficient amount of alumina (Tabel 1), which could reduce the dissolution of silica eliminating the ASR gel formation [50]. Based on a study by Souza and Sanchez [51], they found that samples with 30 wt% FA displayed the lowest expansions, where a high alumina content contributed to ASR mitigation. Similarly, Nguyen et al. [11] reported that due to presence of sufficiently free alumina, the formation of C-A-S-H improved the alkali-binding capacity of the LC3-cement matrix, reducing the mortar expansions.

Overall, 5 wt% CCB ($<100\ \mu\text{m}$, $D_{90} = 34.67\ \mu\text{m}$) exhibited the best ASR mitigation, reducing expansion by 7.2 % and 6.87 % at 28 days and 96 days respectively compared to reference CWG specimens, while the other two biochar had similar ASR expansions when compared to the control group up to 96 days. Phase assemblages of samples exposed to water and NaOH solution will be presented in later sections.

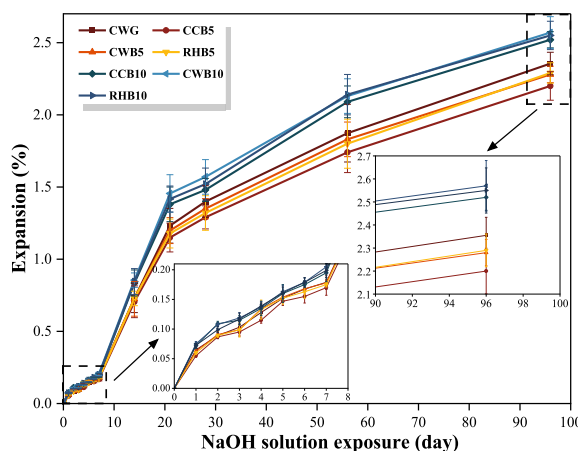


Fig. 4. Mortar bar expansion in AMBT up to 96 days.

3.3. Mass changes

Fig. 5 shows the mass change of samples with and without biochar over the exposure period up to 96 days. Compared with the trend depicted in Fig. 4, similar trend was observed for the mass gain during the exposure period. The results indicated that samples with 10 wt% biochar had higher mass gain than that of the control group. CWB10 had the highest mass increase of 3.32 %, being 9.26 % higher than that of CWG group (3.04 %). Due to relative finer particle size, 4.33 % and 5.97 % increase in the mass gain at 96 days were found in RHB10 and CCB10. The higher mass at 96 days indicated that more sodium ions and water were absorbed in samples with 10 wt% than the control group, revealing higher formations of ASR products.

In terms of samples with 5 wt% biochar, samples with coarser biochar exhibited similar mass gain to the control group, being 2.91 % and 3.24 % reduction for RHB5 and CWB5 group. CCB5 exhibited the lowest mass gain of 2.83 % (6.86 % reduction) among the three groups at 96 days. This finding is consistent with the lowest ASR expansion results (Fig. 4). The presence of finer-size CCB particles improved the hydration process promoting a denser biochar-cement matrix, limiting the access of sodium ions.

3.4. Strength degradation

The effects of biochar with two replacement ratios on the mechanical properties of all mortars up to 96 days are depicted in Fig. 6. It should be mentioned that the mechanical properties were calculated based on the average of three results for all groups. Overall, mortars with 5 wt% biochar exhibited lower mechanical strength degradations when compared to samples with 10 wt% biochar regardless of biochar types up to 96 days. The strength degradation was consistent with the expansion rates shown in Fig. 4.

In terms of compressive strength degradation, after 28-day immersion in water at room temperature or in 1M NaOH bath at 80 °C, CWG had 16.57 % and 27.59 % reduction on 28-day and 96-day compressive strength respectively, acting as the benchmark. CCB5 group displayed the lowest strength degradation of 14.31 % and 25.32 % at 28 days and 96 days respectively. However, higher compressive strength degradations of 17.21–18.28 % (28-day exposure) and 27.81–29.39 % (96-day exposure) were observed for samples with coarser biochar when compared to the compressive strength benchmark. This phenomenon could be due to two main factors: finer-size CCB5 particles exhibited better filler effects providing more hydration sites than coarser biochar (WWB and RHB), refining the porosity of the CCB-cement matrix leading to a higher compressive strength. Secondly, coarser biochar particle experienced cracks after 96-day NaOH solution immersion. Based on SEM images in Fig. 7, a distinct cracking line developed across a RHB particle and surrounding cementitious matrix (Fig. 7a), and multiple cracking lines were observed in a WWB particle (Fig. 7b). It is worth mentioning that the BSE with EDS analysis will be discussed in later sections. Some studies [30,32] reported that although biochar particles provided more hydration sites promoting the strength development of the biochar-cement composites, long-term exposure in aggressive-ion environment led to biochar degradation, forming more accessible channels. After the crack developed across the biochar particle, cracked cementitious matrix would be more susceptible to formations of ASR products. As a result, higher compressive strength reductions were observed in RHB5 and CWB5 group when compared to CWG group. Severe compressive strength degradations were found in mortar samples with 10 wt% biochar, being 21.79–23.24 % and 32.52–36.86 % for the 28-day and 96-day compressive strength respectively. As explained in Section 3.1, excessive biochar particles interfered with the hydration development, reducing the strength gain. Coarser pulverised biochar powder also resulted in a more porous biochar-cement, causing higher strength degradation at long term.

In general, the flexural strength degradations increased with the increasing biochar content (Fig. 6c–d). At 28-day exposure, 7.49–10.76 % and 25.09–29.59 % flexural strength reduction were observed in samples with 5 wt% biochar and 10 wt% biochar respectively when compared to CWG group. However, significant strength degradation (36.51–38.27 %) were found in mortars with 10 wt% biochar. One possible interpretation was that unlike compressive force closed pores in the cementitious matrix, flexural force

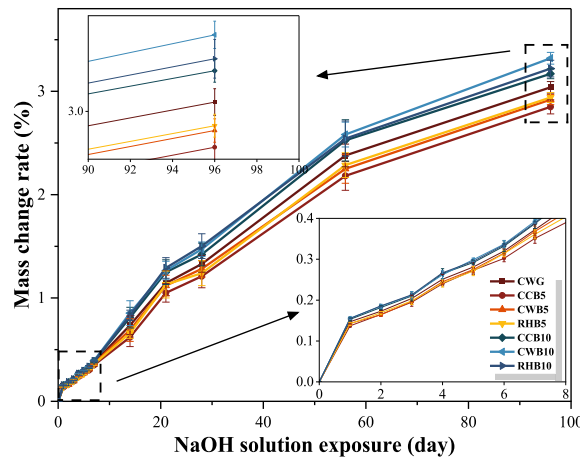


Fig. 5. Mass changes of mortars in 1 NaOH solution bath up to 96 days.

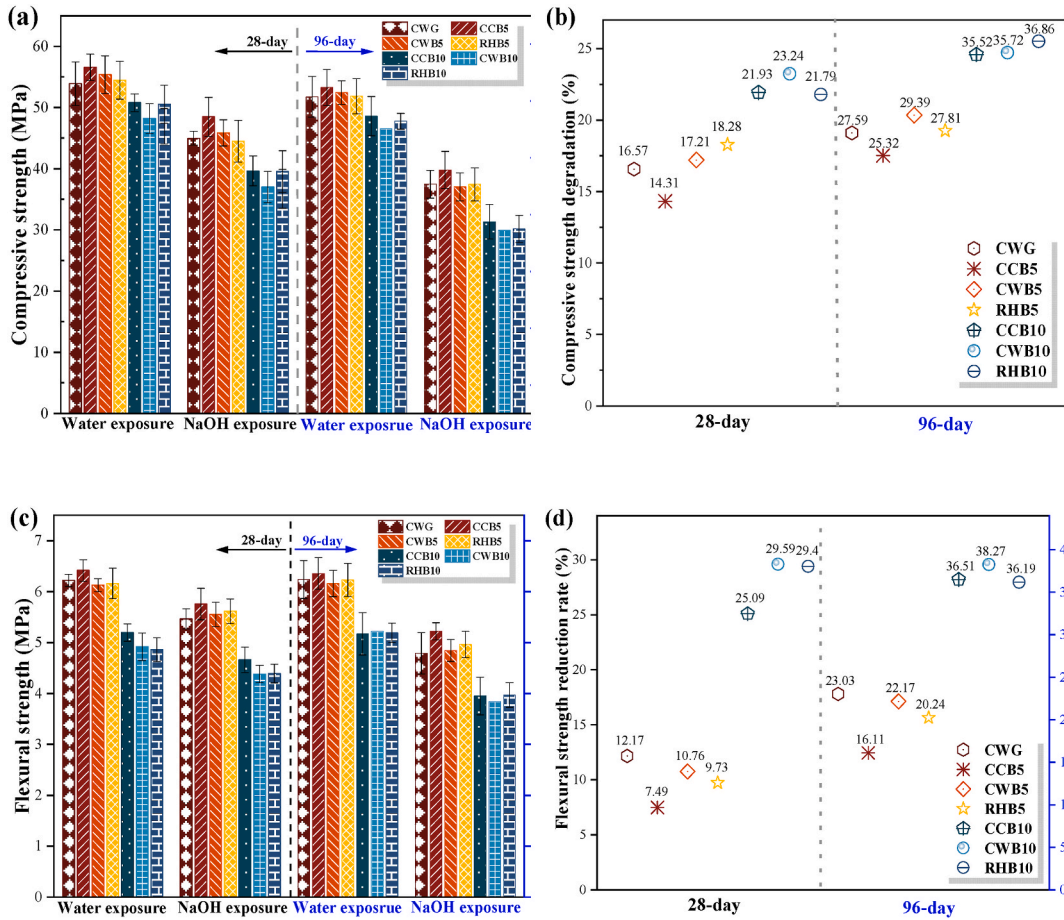


Fig. 6. Mechanical properties of all groups up to 96 days: (a) Compressive strength comparison; (b) Compressive strength degradation; (c) Flexural strength comparison; (d) Flexural strength degradation.

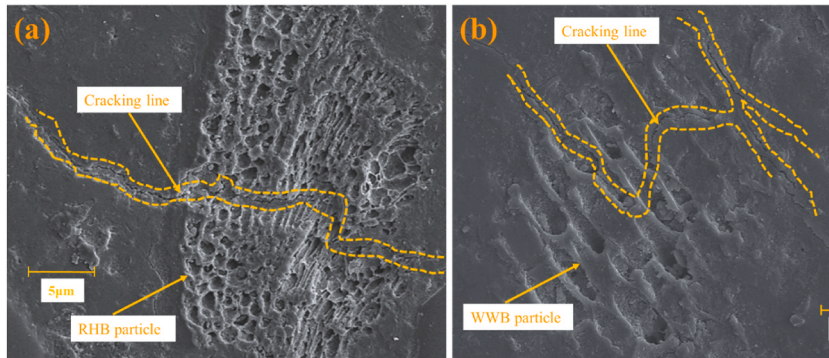


Fig. 7. Typical biochar degradation after 96-day 1M NaOH solution bath: (a) RHB5 group; (b) CWB5 group.

tended to induce cracks in weak area with pores prior to failure of the denser cementitious matrix. After immersing in 1M NaOH solution for 96 days, the combination of excessive porous biochar and ASR-induced cracks lowered the flexural strengths of samples with 10 wt% biochar. Similarly, Boumaaza et al. [52] agreed that excessive biochar powder content leads to weaker tensile plane, reducing the flexural strength.

Overall, by combining the heat development (Fig. 3) and strength degradation (Fig. 6), finer-size corn cob biochar (<100 μm, D90 = 34.67 μm) seemed to be more favourable in resisting sodium-ion ingress, leading to less mechanical strength degradations when compared to the control group and samples with coarse biochar. This finding is in good agreement with the mortar expansion and the

mass change results.

3.5. Phase assemblage

Fig. 8 shows the XRD spectra of all mortars exposed to 1M NaOH solution after 28 days and 96 days. It worth mentioning that waste glass sand was used as main reactive fine aggregates in this study, the diffraction peaks of quartz were relatively higher than other chemical phases (Fig. 8a and b). Thus, the phase change of quartz would not be analysed. A peak accumulation of semi-crystalline ASR gels is observed at $29.4^\circ 2\theta$, indicating the formations of tobermorite-type C-S-H with a layered silicate structure [53–55] and alkali-silicate-hydrates (ASH), including kanemite, makatite, magadiite, kenyaite, shlykovite, and octosilicate [56–58]. Other peaks $31.9^\circ 2\theta$ and $49.9^\circ 2\theta$ revealed the additionally formations of tobermorite-type C-S-H in high-calcium availability. After 96 days of NaOH exposure, higher diffraction peaks of ASR gels were observed, indicating continuous development of alkali-silicate reactions. In addition, the peaks at $12.2^\circ 2\theta$ and $17.4^\circ 2\theta$ indicated the formation of C-A-S-H (zeolite or katoite), where CC5 group exhibited the highest intensity for the two exposure periods.

Overall, lower diffraction peaks of ASR gels were observed in samples with 5 wt% biochar when compared to those of samples with 10 wt% biochar for the two exposure periods in 1M NaOH bath at 80°C . Especially, CCB5 group exhibited the lowest peaks of ASR gels among all samples, highlighting the capacity of finer-size biochar in limiting the ASR expansions. The XRD patterns were consistent with the expansion results, as samples with 10 wt% biochar presented higher expansion due to higher amount of ASR gels. Additionally, the increase of portlandite diffraction peaks and reduction of alite/belite peaks reflected the continuous hydration of all groups in the NaOH bath.

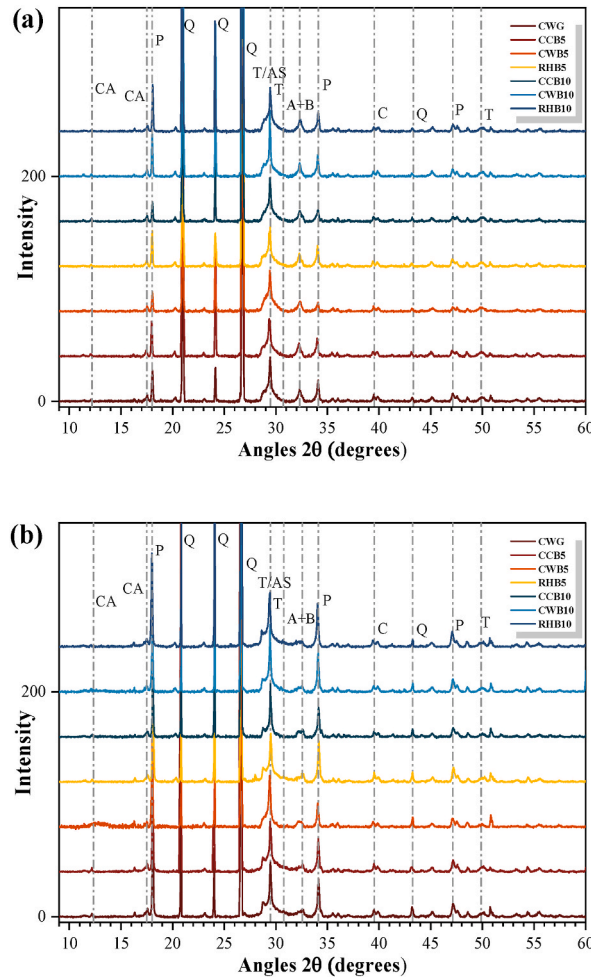


Fig. 8. XRD patterns: (a) 28-day 1M NaOH solution bath; (b) 96-day 1M NaOH solution bath. (Note: A = Alite (C_3S); AS = A-S-H; B = Belite (C_3S); CA = C-A-S-H (zeolite or katoite); CC = Calcite; P = Portlandite; Q = Quartz; T = Tobermorite-type C-S-H).

3.6. TG/DTG analysis

The TG and DTG results of all mortar samples exposed to 28-day and 96-day 1M NaOH solution bath at 80 °C are shown in Fig. 9. The first thermal event in the temperature range of 40–105 °C was attributed to the loss of free or loosely bound water (φ_{water}). The second endothermic peak between 105 and 250 °C was due to the loss of chemical bound water in the ASR gels (φ_{ASR}), including tobermorite-type C-S-H [53,58,59] and ASH [60,61]. Furthermore, the mass loss of tobermorite-type C-S-H might occur in the temperature range of 250–320 °C [58,61]. However, Sinha and Wei [58] reported that since a portion of low-alkali or high-alkali ASR gels might dehydrate in the temperature range of 40–105 °C, leading to an underestimation of the total mass loss of ASR gels. Nevertheless, the quantitative analysis of φ_{water} and φ_{ASR} was calculated based on Eq. (1) and Eq. 2

$$\varphi_{Water} = M_{40} - M_{105} \quad (1)$$

$$\varphi_{ASR} = (M_{105} - M_{250}) + (M_{250} - M_{320}) \quad (2)$$

Fig. 10 shows the mass content of free and loosely bound water and ASR gels after 28-day and 96-day 1M NaOH solution bath at 80 °C respectively. After 28-day NaOH bath, samples with 10 wt% biochar exhibited higher φ_{water} of 4.87–5.02 % than that of samples with 5 wt% biochar (3.36–4.22 %) and CWG group (4.37 %). The lowest φ_{water} (3.36 %) in CCB5 group revealed that the presence of finer-size CCB particle promoted resistance against ion penetrations at 28 days. When the NaOH exposure was extended to 96 days (Fig. 10a), due to the significant ASR product development, the φ_{water} of samples with 10 wt% biochar increased significantly, indicating possible formation of ASR gels dehydrating at low temperature (50 °C–105 °C).

Taking ASR gels mass loss of 4.02 % (the thermal event between 105 °C and 320 °C) in the control group at 28 days as the baseline, a mass loss of 3.72–4.38 % and 4.79–5.26 % were observed in samples with 5 wt% and 10 wt% biochar respectively. In general, using 10 wt% biochar as SCMs led to a slight increase in the formations of ASR products. This phenomenon might be due to a combination of interfered strength development and relative porous biochar-cement matrix. However, due to possible dehydration of small portion of ASR products in the evaporation process of free water and loosely bound water, the ASR gel content would be underestimated. Sinha and Wei [58] emphasised that the overlapping of mass loss calculations in two endothermic events (40 °C–105 °C and 105 °C–320 °C) would lead to direct comparisons being less realistic. Nevertheless, after 96 days of NaOH bath, the mass loss of ASR gels increased for all groups. Only CCB5 and RHB5 exhibited slightly lower ASR gel content than that of the reference group, being in good agreement with mortar expansions and strength degradation analysis.

Overall, TG/DTG results highlighted the possible resistance improvement of finer-size CCB particles, providing proper filler effects and improved hydration development leading to a denser microstructure limiting the ASR gel development.

3.7. BSE-EDS analysis

The BSE images of samples exposed to 96-day 1M NaOH solution bath at 80 °C are depicted in Fig. 11. After 96-day NaOH exposure, different levels of cracks were observed in all groups. In general, samples with 10 wt% biochar exhibited higher amounts of cracks than that of samples with 5 wt% biochar. As shown in Fig. 11e–g, cracks not only penetrated across biochar particles, but also damaged the Interfacial transition zone (ITZ) between biochar and the cementitious matrix (marked along orange dash line), leading to increased susceptibility to ASR development. Biochar degradation was also found in samples with 5 wt% biochar (Fig. 11b–d). This observation revealed the low stability of biochar subjected to long-term 1 M NaOH exposure.

In this study, point of interest (POI) was used to indicate the locations of EDS analysis (Fig. 11), including the paste or hydration products on biochar surface (namely HP, crossing sign), ITZ between the paste and the WGS particle (namely ITZ, circle sign), cracking line in the WGS particle (namely aggregate, triangle sign). Many studies [11,51,53,62] reported that one possible limitation of focused

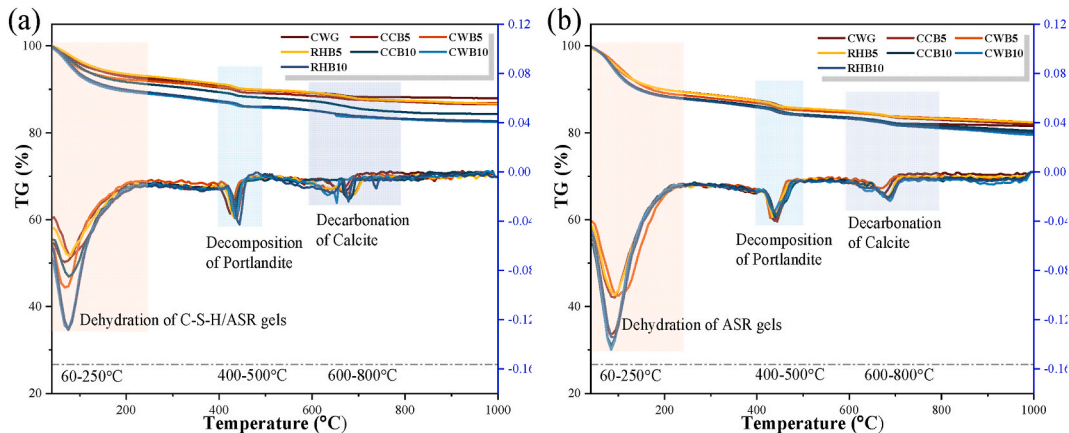


Fig. 9. TG/DTG analysis: (a) 28-day 1M NaOH bath exposure; (b) 96-day 1M NaOH bath exposure.

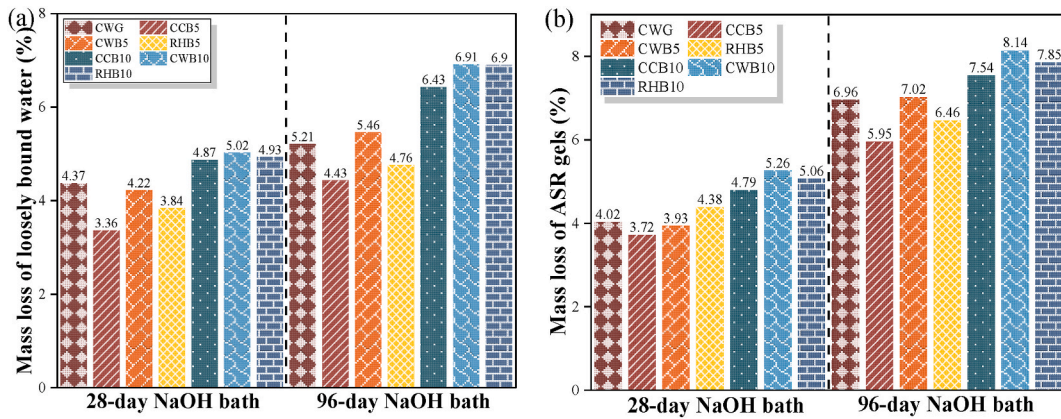


Fig. 10. Mass loss quantitative analysis: (a) Free and loosely bound water; (b) ASR gels.

EDS analysis was that the EDS results could not represent the elemental compositions of the ASR products. Thus, to eliminate the potential negative impacts of focused EDS analysis, 18 points were scanned at each sign, achieving the collection of 100+ points for each group. The elemental analysis of all mortars exposed to 96-day 1M NaOH solution bath at 80 °C are showed in Fig. 12, including (Na + K)-Si-Ca plot and Al-Si-Ca plot. The average values of atomic ratios of 108 points, including Ca/Si, Al/Si, and (Na + K)/Si, are presented in Table 6 (POIs in HP), Table 7 (POIs in ITZ), and Table 8 (POIs in aggregate).

In terms of atomic ratios in HP region, e.g. the cement past or hydration products on biochar surface, (Na + K)/Si ratios of 0.14–0.152 might be due to the formation of small portion of ASR products. CCB5 group exhibited the lowest value of (Na + K)/Si and the highest Ca/Si and Al/Si ratios compared to other groups, indicating possible improvement in the diffusion resistance of alkali ions. The increase in biochar content led to higher (Na + K)/Si ratios and lower Al/Si ratio. This result might highlight the relatively poor resistance of biochar-cement matrix resisting the alkali-ion ingress.

In terms atomic ratios in ASR gel located in the ITZ and cracked line in WGS particle, gradual reductions in Ca/Si ratios were found from the paste to the ITZ and the crack in deep WGS. Similarly, in a study by Deng [63], Ca/Si ratio was 0.367 in the ASR gel near ITZ and 0.327 in the ASR gel deep in WGS. Furthermore, the author also found that various oxides in different glass impacted on the ASR development, where the presence of Cr₂O₃ in green WGP might mitigate the ASR gel development better than in the case of Cr₂O₃-free brown WGP. Ma et al. [64] reported that semi-permeable net of C-S-H gel near aggregate inhibited the access of calcium along the crack to deep aggregate, leading to low Ca/Si ratios during the formation of ASR gel. It should be noted that the average Na/K ratios of ASR gels in ITZ (0.446–0.492) were higher than those of ASR gel in deep aggregate (0.335–0.391). Based on several studies [65,66], crystalline ASR gel exhibited a Na/K ratio being in a range of 0.1–0.27, while amorphous ASR products had Na/K ratio ranging from 0.46 to 0.76. Thus, most of ASR products in ITZ regions for all groups could be considered as amorphous ASR gels, while the ASR gels in deep aggregate cracks could be classified as the combination of amorphous ASR gels and small amount of crystalline ASR gels. Distinct Amorphous ASR products could be observed in BSE image of each group.

Overall, the atomic ratios remained similar reduction or increase trend moving from POIs in the paste to POIs in the crack of deep aggregate for all groups. More discussions will be provided in Section 4.

4. Discussion

Based on aforementioned results and comparisons, different types of biochar exhibited various performances in ASR-induced expansion and strength degradation. According to the available literatures [62,67,68], the formation of ASR products could be divided into three stages: early-age reaction, early-stage expansion (Fig. 13a), and late-stage expansion (Fig. 13b). By adopting this hypothesis, the potential effects of biochar on ASR resistance in WGS-based mortars would be compared and discussed.

4.1. Effects of biochar types

Three biochar were used as SCMs, including CCB (<100 μm, D₉₀ = 34.67 μm), CWB (<239.88 μm, D₉₀ = 79.43 μm) and RHB (<178.48 μm, D₉₀ = 69.18 μm). Fig. 13 shows the performance comparison of mortars with and without biochar after 28-day and 96-day 1M NaOH bath at 80 °C. By replacing cement up to 5 wt%, only slight heat increase was found in CCB5 groups, while the other two groups had similar heat when comparing to the control group (Fig. 13). CCB5 group exhibited improved hydration process, leading to higher mechanical properties among all groups (Fig. 6). As a result, lowest mortar expansion and mass gain was observed in CCB5 group at the early-age reaction stage, where CCB5 group might experience a lower ASR gels development. However, no significant differences were found for other samples, having similar increasing trend of mortar expansions and mass gain.

As the NaOH solution exposure time increased, slight reductions in mortar bar expansion (4.2–7.2 %) at 28 days were observed in samples with 5 wt% biochar when compared to the reference group (Fig. 13a). The differences should be attributed to the strength development and the biochar-cement matrix. As reported by Gupta et al. [43], ultra-fine biochar (<10 μm, D₉₀ = 9 μm) led to

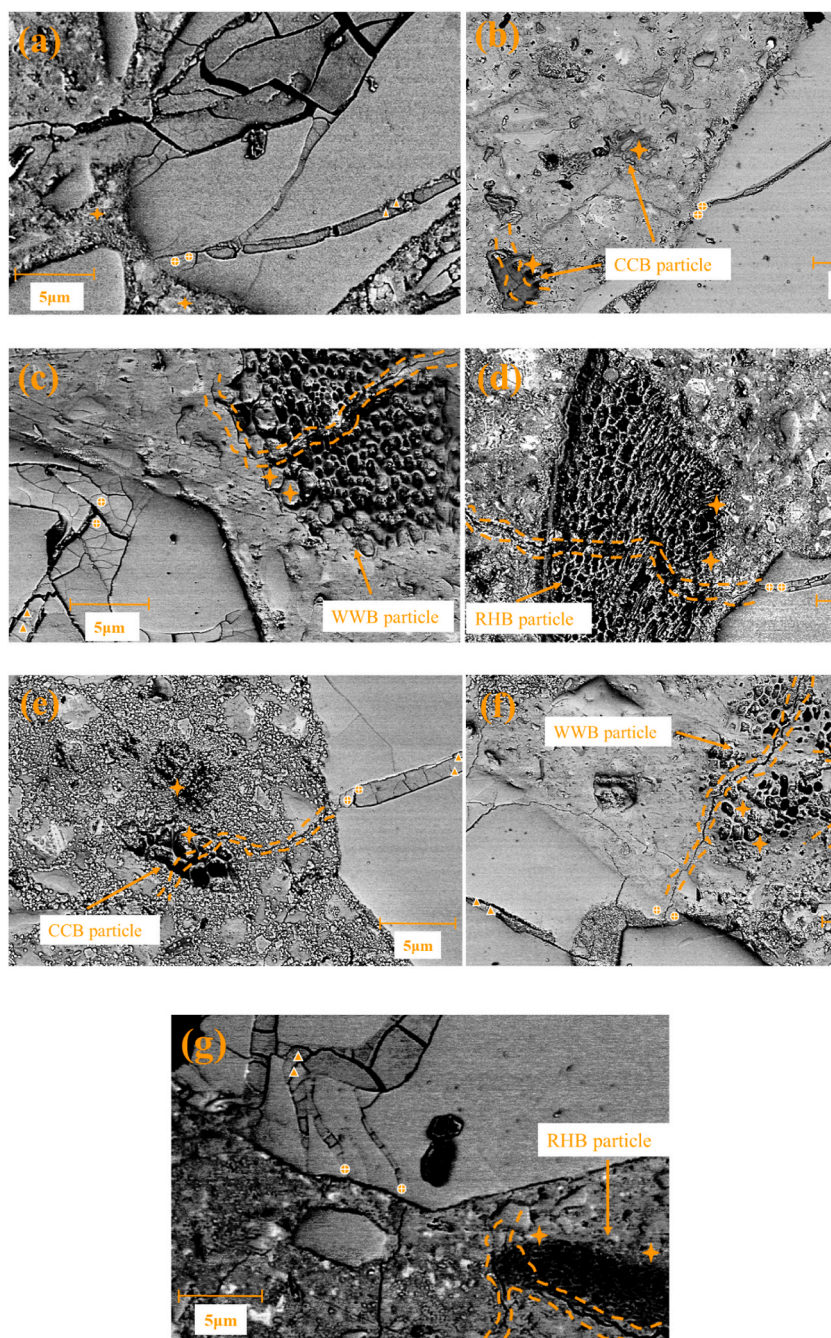


Fig. 11. BSE images with POIs of all samples after 96-day 1M NaOH solution bath: (a) CWG group; (b) CCB5 group; (c) CWB5 group; (d) RHB5 group; (e) CCB10 group; (f) CWB10 group; (g) RHB10 group. (Note: Crossing sign reflects POIs in cementitious matrix or hydration products in biochar surface; Cycle sign is POIs in edge of WGS (ITZ); Triangle sign donates POIs in the ASR-induced crack in WGS particle).

significant heat increase, indicating higher strength gain with a refined microstructure. However, considering the size differences among the three biochar, CWB and RHB were relatively coarser, inevitably interfering with the strength development and initiating more accessible channels for sodium ion diffusion. On the other hand, it should be pointed out that the porosity of the CCB-cement matrix would be less than that of other two groups with biochar addition. During the early-stage expansion, although biochar addition provided filler effects in pores of the cementitious matrix, alkali ions and water molecules could access through coarse biochar particles penetrating to deeper cementitious matrix, leading to slight reduction of mortar expansion after 28-day of NaOH exposure. During the stage, since the cementitious matrix did not severely damaged, the formation of ASR gels was restricted due to less availability of alkali ions. Noticeably reductions in expansion and mass gain rate were observed between for CCB5 group (Figs. 5 and 6)

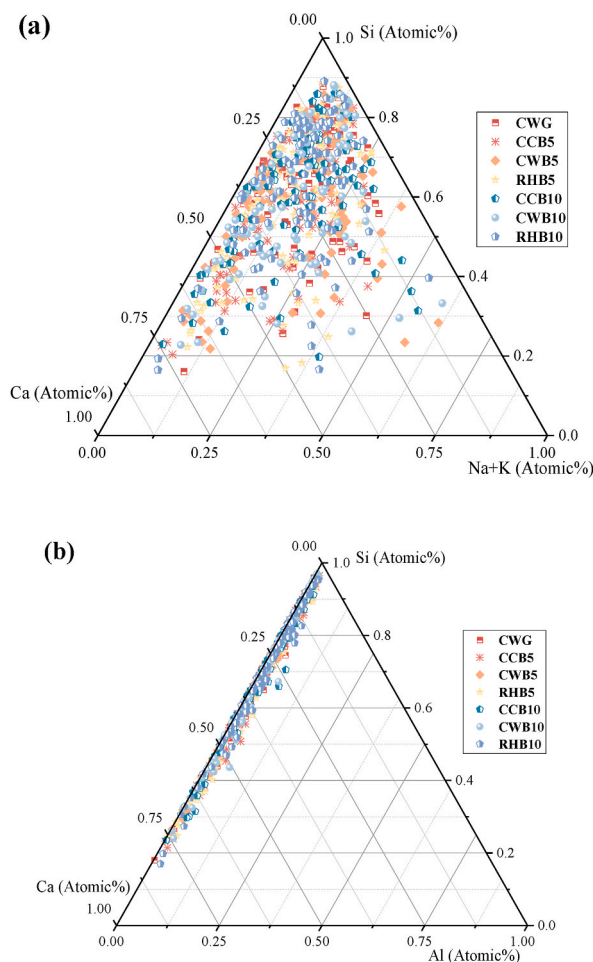


Fig. 12. Ternary plots of elemental compositions in hydration products and ASR gels: (a) (Na + K)-Si-Ca plot; (b) Al-Si-Ca plot.

Table 6

Elemental analysis of hydration products in the paste or on biochar surface (HP).

	(Na + K)/Si		Ca/Si		Al/Si	
	Average	STVD	Average	STVD	Average	STVD
CWG	0.147	0.154	0.899	0.867	0.018	0.017
CCB5	0.140	0.089	0.953	0.889	0.024	0.020
CWB5	0.145	0.115	0.942	0.735	0.017	0.014
RHB5	0.143	0.105	0.933	0.795	0.021	0.019
CCB10	0.145	0.101	0.908	0.730	0.016	0.022
CWB10	0.152	0.114	0.925	0.667	0.017	0.019
RHB10	0.146	0.123	0.911	1.045	0.016	0.027

when compared to control group. CCB5 group also exhibited the lowest mass loss of ASR gel after 28-day of NaOH exposure (Fig. 10).

However, due to the presence of numerous ASR-induced cracks, all groups exhibited significant expansions and mass gain after 96-day of NaOH exposure (Fig. 13b). The ASR development was highly related to the characteristics of the biochar-cement matrix. Based on BSE images in Fig. 11, cracks could be observed crossing biochar particle, revealing the degradation of biochar after severe ASR development. This phenomenon indicated the ASR-induced cracks have extended from deep or ITZ of reactive glass sand to the cementitious matrix. Based on the elemental analysis in Tables 7 and 8, (Na + K) ratio of ASR gels in CWB5 group was higher than that of the control group in both ITZ and deep aggregate regions. Na/K ratio also indicated the major formation of amorphous ASR gels in two POIs. Higher content of ASR gels (Fig. 10) was formed due to relatively porous CWB-cement matrix. Furthermore, direct evidence could be seen in Figs. 6 and 13, where the mechanical degradations in samples with 5 wt% biochar were more severe at 96 days than those at 28 days of NaOH exposure. As a result, the addition of 5 wt% biochar led to only slight improvement in resistance against ASR

Table 7

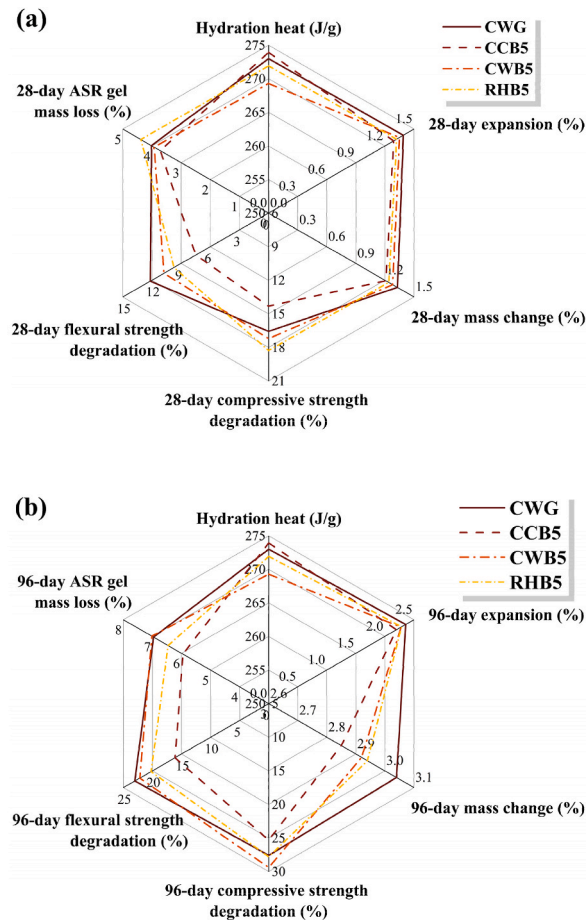
Elemental analysis of ASR gels in ITZ zone between paste and WGS (ITZ).

	(Na + K)/Si		Ca/Si		Al/Si		Na/K	
	Average	STVD	Average	STVD	Average	STVD	Average	STVD
CWG	0.418	0.317	0.498	0.369	0.017	0.012	0.471	0.314
CCB5	0.375	0.308	0.556	0.529	0.021	0.020	0.446	0.524
CWB5	0.435	0.519	0.519	0.555	0.018	0.016	0.492	0.384
RHB5	0.417	0.450	0.532	0.678	0.020	0.023	0.454	0.510
CCB10	0.432	0.459	0.492	0.456	0.020	0.025	0.475	0.346
CWB10	0.470	0.465	0.447	0.417	0.018	0.025	0.465	0.582
RHB10	0.437	0.497	0.496	0.495	0.019	0.018	0.458	0.472

Table 8

Elemental analysis of ASR gels in cracks of WGS (Aggregate).

	(Na + K)/Si		Ca/Si		Al/Si		Na/K	
	Average	STVD	Average	STVD	Average	STVD	Average	STVD
CWG	0.255	0.180	0.259	0.271	0.014	0.019	0.391	0.421
CCB5	0.261	0.147	0.275	0.200	0.018	0.018	0.347	0.358
CWB5	0.287	0.275	0.242	0.203	0.012	0.014	0.386	0.215
RHB5	0.261	0.235	0.264	0.345	0.014	0.017	0.368	0.351
CCB10	0.289	0.245	0.234	0.203	0.015	0.015	0.335	0.472
CWB10	0.321	0.182	0.238	0.211	0.013	0.017	0.358	0.381
RHB10	0.290	0.224	0.260	0.239	0.016	0.018	0.349	0.294

**Fig. 13.** Mortars performance comparison: (a) 28-day NaOH solution exposure; (b) 96-day NaOH solution exposure.

expansion (Fig. 5).

Due to the combination of finer-size CCB particle and a denser microstructure in CCB-cement matrix, lower amount of cracking lines were observed with the same magnification of $200\times$, reflecting lower portion of ASR products. Overall, by considering the ASR expansion, mass gain and strength degradation after 96 days of 1M NaOH bath at 80°C (Fig. 13a and b), finer-size corn cob biochar seemed to provide a better mitigation of ASR when compared to coarser-size waste wood biochar and rice husk biochar.

In general, the potential of SCMs in mitigating ASR development is affected by the Ca/Si ratio of the ASR gels and the availability of the alumina [11,51,69,70]. Based on a study by Nguyen et al. [11], ASR gels with high calcium content demonstrated lower swelling capacity. Several studies [71–73] also reported that ASR gels with high Ca/Si (>0.5) displayed high stiffness with low expansion. Based on Tables 7 and 8, the Ca/Si ratios of samples (0.519–0.556) with 5 wt% biochar were slightly higher than that of the reference group, being in good agreement with the slight mortar bar expansion reductions at 96 days. However, a negligible difference in Ca/Si ratios were observed for samples with and without biochar, having similar expansions after 96 days. In terms of role of alumina, Al^{3+} could react with alkali ions to form lower-solubility phases, e.g. zeolite (C-A-S-H), K-A-S-H or N-A-S-H, mitigating the ASR process [11,70,74]. Another interpretation is that the presence of aluminium in the silica framework leads to reduction of Si dissolution rate with lower interfacial free energy, thus eliminating the formations of ASR gels [11]. By considering this favourable benefit of alumina, XRF results in Table 2 exhibit that the value of Al_2O_3 of three biochar was 12.83 %, 3.95 %, and 5.78 % for CCB, WWB and RHB respectively. As a result, insufficient supply of aluminium ions did not contribute to effective chemical adsorption effect of aluminium ions, in which the adsorption of Al ions on the surface of amorphous silicon led to negative charging sites, preventing the dissolution of silicon in alkaline environment to reduce ASR. Based on Fig. 12 and Tables 7 and 8, the ASR gels of CCB5 had slightly higher Al/Si ratio than that of the control group, possibly contributing to the slight reductions of ASR process up to 96 days. Furthermore, Deng et al. [75] reported that samples with lithium nitrate exhibited lower content of ASR gel when compared to lithium-free mortar. The author revealed that, similar to Al ions, lithium ions could bind with negative charges of silica layers, mitigating the formation of ASR gels. However, due to no or limited supply of Al and Li ions, fine-size biochar led to only limited improvement in the ASR mitigation.

Based on the above-mentioned comparisons, the role of various biochar in mitigating ASR process includes different aspects. Firstly, finer-size biochar exhibited better ASR mitigation, by improving the cement hydration and lowering the strength degradation. The application of 5w% of corn cob biochar ($<100\text{ }\mu\text{m}$, $\text{D}_{90} = 34.67\text{ }\mu\text{m}$) led to the lowest mortar bar expansion and mass gain among all groups. Secondly, the free alumina content of the binder, supplying aluminium ions plays a crucial role in mitigating ASR. However, aluminium ions supply by biochar is very limited due to their low alumina content (Table 1), leading to a poor surface passivation of reactive aggregate not able to prevent the dissolution of amorphous silicon. As a result, ASR mitigation effect remained very limited. Noticeably, the alumina content was the highest in corn cob biochar CCB (Table 1), which can also explain the slightly better performance of mortar specimens with 5w% of CCB in mitigation ASR. Overall, 5 wt% finer-size CCB can slightly improve both mechanical properties and ASR resistance. 5 wt% coarser-size waste wood biochar and rice husk biochar could still be used as a sustainable component, having similar ASR-resisting capacity than the control group.

4.2. Effects of cement replacing ratio

Samples with 10 wt% biochar had higher mortar bar expansions and mass gain, while experiencing higher mechanical strength degradations at 96 days when compared to samples with 5 wt% biochar. This result showed opposite conclusion compared to other types of SCMs [69,70], where 20–30 wt% limestone and calcined clay [11], 30 wt% FA [74,76] and 20 wt% slag [47,77] could be used in GPC system to mitigate ASR process.

Considering the characteristics of biochar (Fig. 1), biochar exhibited a porous microstructure when compared to FA, clay, or slag having solid texture. In terms of higher cement replacing percentages, e.g. 10 wt% to 20 wt% FA, clay or slag, finer-size solid powder could provide direct filler effects in pores of the cementitious matrix, reducing the overall porosity of samples with such SCMs. However, due to the porous microstructure of biochar, although more hydration sites could improve the early hydration, direct exposure to 1M NaOH solution negatively impacted the mortar microstructure. Moreover, this phenomenon was highly related to its particle size, where ultra-fine particles had predominant improvement of cement hydration. Thus, the use of ultra-fine biochar showed proper potential of higher cement replacement percentages, which is strongly recommended for future studies. Based on BSE images of samples at 96 days, numerous cracks were observed in samples with 10 wt% biochar, where the degradation of coarser-size biochar led to improved susceptibility to ASR development, posing another challenge of using coarse biochar with large size in resisting the development of ASR process.

Overall, 10 wt% finer-size corn cob biochar could be conservatively used as cement replacement, with comparable ASR resistance when compared to the control group. One possible solution for higher ASR mitigation was to utilise even finer-size CCB or other types of biochar, e.g. biochar size being less than $40\text{ }\mu\text{m}$ or even ultra-fine size ($<10\text{ }\mu\text{m}$), where improved hydration development and less porous biochar-cement matrix could be expected to have better resistance against ASR development up to 96 days of AMBT test.

5. Limitations

This study adopted only the Accelerated Mortar Bar Test (AMBT) as per ASTM C1260-23 [37]. Real-world applications are highly required to compare the experimental results of biochar in slightly mitigating the ASR process. As a pioneering study of exploring potential role of using biochar to improve the ASR resistance of the biochar-cement composites, only three biochar were used. Thus, it is recommended to further validate the effects of fine-size or ultra-fine-size biochar as well as the content of alumina in biochar powder on the potential resistance improvement against the ASR process. Therefore, a more comprehensive understanding of how biochar

would act in mitigating the ASR development could be explained, improving the practicality of biochar as SCMs in the construction sector.

6. Conclusions

This study investigates the effects of three biochar, including corn cob biochar (CCB), waste wood biochar (CWB), and rice husk biochar (RHB) on the ASR mitigation in sustainable waste glass sand-based mortars using the Accelerated Mortar Bar Test (AMBT). The major conclusions were drawn as the follows.

- 1) Due to its finer particle size ($<100\ \mu\text{m}$, $D_{90} = 34.67\ \mu\text{m}$), CCB5 group exhibited the highest hydration heat among all WGS-cement mortars. After 96-day of exposure in 1M NaOH bath at $80\ ^\circ\text{C}$, CCB5 had the lowest mortar bar expansion and mass gain, while demonstrating the lowest mechanical strength degradation.
- 2) XRD patterns revealed increased intensity of ASR gels, including tobermorite-type C-S-H and ASH in all groups from 28-day to 96-day NaOH exposure. Small diffraction peaks of C-A-S-H (zeolite or katoite) were observed in CCB5, indicating the possible contribution of C-A-S-H in mitigating the ASR development.
- 3) TG/DTG analysis further demonstrated the role of CCB powder in mitigating the formation of ASR products, where the lowest mass loss of ASR gels in a temperature range from 105 to $320\ ^\circ\text{C}$ was found.
- 4) BSE images revealed the degradation of biochar particles due to severe ASR-induced cracks. The values of Ca/Si ratio gradually reduced from POIs in paste or hydration products on biochar to POIS in aggregate cracks. Amorphous ASR gels were identified in the ITZ between the WGS and the paste, while a combination of amorphous and crystalline ASR gels was observed based on lower Na/K ratio.
- 5) Up to 10 wt% CCB ($<100\ \mu\text{m}$, $D_{90} = 34.67\ \mu\text{m}$) could be conservatively used as SCM, demonstrating comparable ASR-resisting performance when compared to the reference group.
- 6) The novelty of this work was to comprehensively analyse the role of different biochar in the ASR-resisting performances of WGS-based mortars using the AMBT, where mortar bar expansion, mass gain, and strength degradation was compared up to 96 days. Finer-size biochar (size $\leq 100\ \mu\text{m}$) could be conservatively used up to 5 wt% as cement replacement.
- 7) However, it is highly recommended that more studies need to be performed to investigate the role of ultra-fine biochar with higher cement replacing ratio, further improving the sustainability of the biochar-cement composites.

CRediT authorship contribution statement

Xuqun Lin: Writing – original draft, Visualization, Validation, Methodology, Investigation, Formal analysis, Data curation, Conceptualization. **Tianxing Shi:** Writing – original draft, Visualization, Validation, Investigation, Formal analysis, Data curation, Conceptualization. **Quang Dieu Nguyen:** Writing – review & editing, Validation, Supervision, Project administration, Methodology, Investigation, Conceptualization. **Arnaud Castel:** Writing – review & editing, Supervision, Project administration, Investigation, Funding acquisition, Conceptualization. **Vivian W.Y. Tam:** Writing – review & editing, Investigation.

Declaration of competing interest

The authors declare that they have no known competing financial interests or personal relationships that could have appeared to influence the work reported in this paper.

Acknowledgements

The authors highly appreciate Australian Research Council, Australia (DP220101051) and all assistances from University of Technology Sydney Research Academic Program at Tech Lab (UTS RAPT).

Data availability

Data will be made available on request.

References

- [1] W. Liu, S. Tan, L. Qing, Y. Li, Pozzolanic activity of biochar with high carbon content and its influence on comprehensive strength-emission performance of biochar-cement composite paste, *Constr. Build. Mater.* 478 (2025) 141427.
- [2] R.G. Pillai, R. Gettu, M. Santhanam, S. Rengaraju, Y. Dhandapani, S. Rathnarajan, A.S. Basavaraj, Service life and life cycle assessment of reinforced concrete systems with limestone calcined clay cement (LC3), *Cement Concr. Res.* 118 (2019) 111–119.
- [3] S.A. Miller, V.M. John, S.A. Pacca, A. Horvath, Carbon dioxide reduction potential in the global cement industry by 2050, *Cement Concr. Res.* 114 (2018) 115–124.
- [4] M.S. Imbabi, C. Carrigan, S. McKenna, Trends and developments in green cement and concrete technology, *Int. J. Sustain. Built Environ.* 1 (2) (2012) 194–216.
- [5] Q. Zhang, B. Liu, Z. Sun, Q. Li, S. Wang, X. Lu, J. Liu, S. Zhang, Preparation and hydration process of copper slag-granulated blast furnace slag-cement composites, *Constr. Build. Mater.* 421 (2024) 135717.
- [6] Z. Giergiczny, Fly ash and slag, *Cement Concr. Res.* 124 (2019) 105826.

- [7] J. Liu, X. Gao, T. Chen, M. Sun, Y. Ou, X. Ji, A novel strategy to improve the early age strength of high-volume fly ash cement pastes: the combination of seawater and calcined layered double hydroxides as an innovative chemical activator, *Constr. Build. Mater.* 473 (2025) 141038.
- [8] W. Chen, L. Chen, S. Yin, Effect of bacteria on cemented fly-ash backfill: mechanical strength, hydration mechanism and leaching behavior, *Constr. Build. Mater.* 472 (2025) 140791.
- [9] M. Zubair, N.D. Mu'azu, M. Nasir, M.S. Manzar, M.A. Aziz, M. Saleem, M.A. Al-Harthi, Cellulose nanocrystals from office paper waste for green mortar: process optimization modeling, characterization, and mechanical properties, *Arabian J. Sci. Eng.* 47 (4) (2022) 5377–5393.
- [10] M.A. Aziz, M. Zubair, M. Saleem, Development and testing of cellulose nanocrystal-based concrete, *Case Stud. Constr. Mater.* 15 (2021) e00761.
- [11] Q.D. Nguyen, T. Kim, A. Castel, Mitigation of alkali-silica reaction by limestone calcined clay cement (LC3), *Cement Concr. Res.* 137 (2020) 106176.
- [12] S.D.C. Gomes, Q.D. Nguyen, W. Li, A. Castel, Shrinkage and carbonation of alkali-activated calcined clay-ground granulated blast furnace slag (GGBFS) concrete, *Cement Concr. Res.* 194 (2025) 107899.
- [13] J. Sun, P. Zhang, Effects of different composite mineral admixtures on the early hydration and long-term properties of cement-based materials: a comparative study, *Constr. Build. Mater.* 294 (2021) 123547.
- [14] J.O. Ukpatha, P.A.M. Basheer, L. Black, Slag hydration and chloride binding in slag cements exposed to a combined chloride-sulphate solution, *Constr. Build. Mater.* 195 (2019) 238–248.
- [15] M. Teymouri, M. Shakouri, Chloride desorption mechanisms of cement pastes containing fly ash, *Constr. Build. Mater.* 370 (2023) 130667.
- [16] X. Li, Y. Fan, Q. Li, S.P. Shah, Experimental study on early-age fracture behavior of cement mortar with the addition of fly ash, *Constr. Build. Mater.* 465 (2025) 140255.
- [17] F. Zunino, K. Scrivener, Microstructural developments of limestone calcined clay cement (LC3) pastes after long-term (3 years) hydration, *Cement Concr. Res.* 153 (2022) 106693.
- [18] P. Ye, B. Guo, H. Qin, C. Wang, J. Li, Y. Chen, D. Lu, L. Wang, P. Gao, P. Ma, B. Zhan, Q. Yu, Investigation of the properties and sustainability of modified biochar-doped cement-based composite, *Cement Concr. Compos.* 153 (2024) 105684.
- [19] X. Lin, Q.D. Nguyen, A. Castel, P. Li, W.V.Y. Tam, W. Li, Self-healing efficiency of sustainable biochar-cement composites incorporating crystalline admixtures, *Constr. Build. Mater.* 458 (2025) 139542.
- [20] T.S. Bhagat, R.K. Pancharathi, Performance, microstructure and carbon sequestration potential of agro biochar based cement mortars, *Cement Concr. Compos.* 156 (2025) 105867.
- [21] D. Kalderis, E. Anastasiou, E. Petrakis, S. Konopisi, Utilization of biochar from olive tree pruning as additive to cement mortars, *J. Clean. Prod.* 469 (2024) 143137.
- [22] X. Lin, W. Li, Y. Guo, W. Dong, A. Castel, K. Wang, Biochar-cement concrete toward decarbonisation and sustainability for construction: characteristic, performance and perspective, *J. Clean. Prod.* 419 (2023) 138219.
- [23] X. Jiang, F. Qu, Y. Zhang, X. Zhu, A.Y.F. Leung, C.S. Poon, D.C.W. Tsang, Cold-bonded biochar-cement lightweight aggregates for evaporation-enhanced permeable bricks, *J. Clean. Prod.* 493 (2025) 144886.
- [24] Y. Tang, J. Qiu, CO₂-sequestering ability of lightweight concrete based on reactive magnesia cement and high-dosage biochar aggregate, *J. Clean. Prod.* 451 (2024) 141922.
- [25] X. Ying, X. Zhao, M. Ye, C. Wang, B. Zhan, J. Zhao, Z. He, X. Nie, Waste rice straw biochar recycled concrete: carbon sequestration, durability and microstructure, *J. Clean. Prod.* 512 (2025) 145690.
- [26] S. Gupta, H.W. Kua, C.Y. Low, Use of biochar as carbon sequestering additive in cement mortar, *Cement Concr. Compos.* 87 (2018) 110–129.
- [27] M.A. Aziz, M. Zubair, M. Saleem, Y.M. Alharthi, N. Ashraf, K.S. Alotaibi, O. Aga, A.A.A. Al Eid, Mechanical, non-destructive, and thermal characterization of biochar-based mortar composite, *Biomass Convers. Biorefin.* (2023).
- [28] Z. Kang, Y. Yang, J. Zhang, N. Li, Synergistic effects of biochar and carbon black on conductive cement composites: mechanical and conductive properties, *Constr. Build. Mater.* 470 (2025) 140579.
- [29] L. Mo, J. Fang, B. Huang, A. Wang, M. Deng, Combined effects of biochar and MgO expansive additive on the autogenous shrinkage, internal relative humidity and compressive strength of cement pastes, *Constr. Build. Mater.* 229 (2019) 116877.
- [30] S. Gupta, S. Muthukrishnan, H.W. Kua, Comparing influence of inert biochar and silica rich biochar on cement mortar – hydration kinetics and durability under chloride and sulfate environment, *Constr. Build. Mater.* 268 (2021) 121142.
- [31] W. Xu, Y. Zhang, M. Li, F. Qu, C.S. Poon, X. Zhu, D.C.W. Tsang, Durability and micromechanical properties of biochar in biochar-cement composites under marine environment, *J. Clean. Prod.* 450 (2024) 141842.
- [32] X. Lin, Q.D. Nguyen, A. Castel, Y. Pang, Z. Deng, T. Shi, W. Li, V.W.Y. Tam, Durability of biochar-cementitious composites incorporating crystalline admixture in chloride and sulphate environments, *Constr. Build. Mater.* 458 (2025) 139554.
- [33] Z. Deng, S. Zhang, Z. Deng, PVA fiber-reinforced geopolymer mortar made with hybrid recycled aggregates: toward thermal insulation, lightweight and improved durability, *J. Clean. Prod.* 426 (2023) 139200.
- [34] Y. Jiao, Y. Zhang, M. Guo, L. Zhang, H. Ning, S. Liu, Mechanical and fracture properties of ultra-high performance concrete (UHPC) containing waste glass sand as partial replacement material, *J. Clean. Prod.* 277 (2020) 123501.
- [35] X. Liu, Z. Ye, J.-X. Lu, S. Xu, S.-C. Hsu, C.S. Poon, Comparative LCA-MCDA of high-strength eco-pervious concrete by using recycled waste glass materials, *J. Clean. Prod.* 479 (2024) 144048.
- [36] Y. Wang, X. Fan, R. Wu, H. Lin, W. Feng, Experimental study on long-term impermeability of recycled aggregate concrete mixed with crystalline admixture and waste glass powder, *J. Clean. Prod.* 458 (2024) 142551.
- [37] A.S.f. Testing, M.C.C.-o. Cement, ASTM C1260-23 Standard Test Method for Potential Alkali Reactivity of Aggregates (Mortar-Bar Method), ASTM International, 2023.
- [38] A.S.f. Testing, M.C.C.-o. Cement, ASTM C109-20: Standard Test Method for Compressive Strength of Hydraulic Cement Mortars, ASTM International, 2020.
- [39] A.S.f. Testing, M.C.C.-o. Cement, ASTM C348-21: Standard Test Method for Flexural Strength of Hydraulic-Cement Mortars, ASTM International, 2013.
- [40] K. Scrivener, R. Snellings, B. Lothenbach, A Practical Guide to Microstructural Analysis of Cementitious Materials, first ed., CRC Press, 2016.
- [41] P. Li, W. Li, K. Wang, J.L. Zhou, A. Castel, S. Zhang, S.P. Shah, Hydration of Portland cement with seawater toward concrete sustainability: phase evolution and thermodynamic modelling, *Cement Concr. Compos.* 138 (2023) 105007.
- [42] P. Zhan, J. Wang, H. Zhao, W. Li, S.P. Shah, J. Xu, Impact of synthetic C-S-H seeds on early hydration and pore structure evolution of cement pastes: a study by ¹H low-field NMR and path analysis, *Cement Concr. Res.* 175 (2024) 107376.
- [43] S. Gupta, P. Krishnan, A. Kashani, H.W. Kua, Application of biochar from coconut and wood waste to reduce shrinkage and improve physical properties of silica fume-cement mortar, *Constr. Build. Mater.* 262 (2020) 120688.
- [44] A. Dixit, A. Verma, S.D. Pang, Dual waste utilization in ultra-high performance concrete using biochar and marine clay, *Cement Concr. Compos.* 120 (2021) 104049.
- [45] J. Zhang, G. Wei, D. Yang, S. Yang, X. Wang, J. Li, J. Yang, M. Song, Z. Liu, W. Wang, Y. Mao, Investigation of sludge-based iron-biochar material derived for cement: composites performance, hydration mechanism, and sustainability, *Constr. Build. Mater.* 474 (2025) 141099.
- [46] C. Zhang, A. Wang, Effect of mineral admixtures on alkali-silica reaction, *J. Wuhan Univ. Technol.-Materials Sci. Ed.* 23 (1) (2008) 16–19.
- [47] C. Karakurt, İ.B. Topçu, Effect of blended cements produced with natural zeolite and industrial by-products on alkali-silica reaction and sulfate resistance of concrete, *Constr. Build. Mater.* 25 (4) (2011) 1789–1795.
- [48] K. Turk, C. Kina, M. Bagdiken, Use of binary and ternary cementitious blends of F-Class fly-ash and limestone powder to mitigate alkali-silica reaction risk, *Constr. Build. Mater.* 151 (2017) 422–427.
- [49] A. Joshaghani, The effect of trass and fly ash in minimizing alkali-carbonate reaction in concrete, *Constr. Build. Mater.* 150 (2017) 583–590.
- [50] T. Chappex, K.L. Scrivener, The influence of aluminium on the dissolution of amorphous silica and its relation to alkali silica reaction, *Cement Concr. Res.* 42 (12) (2012) 1645–1649.

- [51] D.J. De Souza, L.F.M. Sanchez, Evaluating the efficiency of SCMs to avoid or mitigate ASR-induced expansion and deterioration through a multi-level assessment, *Cement Concr. Res.* 173 (2023) 107262.
- [52] M. Boumaaza, A. Belaadi, M. Bourchak, M. Jawaid, S. Hamid, Comparative study of flexural properties prediction of *Washingtonia filifera* rachis biochar bio-mortar by ANN and RSM models, *Constr. Build. Mater.* 318 (2022) 125985.
- [53] D. Luo, A. Sinha, R. Mulcahy, J. Wei, Influence of enforced carbonation on alkali-silica reaction: performance and multi-scale mechanisms, *Cement Concr. Compos.* 153 (2024) 105721.
- [54] X. Hou, L.J. Struble, R.J. Kirkpatrick, Formation of ASR gel and the roles of C-S-H and portlandite, *Cement Concr. Res.* 34 (9) (2004) 1683–1696.
- [55] X. Hou, R.J. Kirkpatrick, L.J. Struble, P.J.M. Monteiro, Structural investigations of Alkali Silicate gels, *J. Am. Ceram. Soc.* 88 (4) (2005) 943–949.
- [56] T. Honorio, W. Wei, Atomic structure of nanocrystalline and amorphous ASR products, *Cement Concr. Res.* 181 (2024) 107521.
- [57] G.D. Guthrie, J.W. Carey, A thermodynamic and kinetic model for paste–aggregate interactions and the alkali–silica reaction, *Cement Concr. Res.* 76 (2015) 107–120.
- [58] A. Sinha, J. Wei, Phase, structure, and hygroscopic property evolutions of alkali-silica reaction gels under freeze drying, *Cement Concr. Res.* 186 (2024) 107692.
- [59] M. Földvári, Handbook of Thermogravimetric System of Minerals and its Use in Geological Practice, Geological Institute of Hungary, Budapest, 2011.
- [60] R.J. Kirkpatrick, A.G. Kalinichev, X. Hou, L. Struble, Experimental and molecular dynamics modeling studies of interlayer swelling: water incorporation in kanemite and ASR gel, *Mater. Struct.* 38 (4) (2005) 449–458.
- [61] G.G. Almond, A Nuclear Magnetic Resonance Study of Hydrous Layer Silicates, 1995.
- [62] W. Wang, S. Zhang, Y. Zhang, T. Noguchi, I. Maruyama, Understanding the influence of slag fineness and water-to-binder ratio on the alkali-silica reaction in alkali-activated slag mortars, *Cement Concr. Compos.* 157 (2025) 105907.
- [63] Z. Deng, Utilisation of steel fibres to reinforce waste glass concrete: Alkali–silica reaction, engineering properties, and 3D mesoscale modelling, *Case Stud. Constr. Mater.* 17 (2022) e01686.
- [64] P. Ma, J. Li, J. Bai, Y. Zhuo, L. Chi, Y. Zhu, Z. Shi, H. Ma, G. Chen, Effect of type and quantity of inherent alkali cations on alkali-silica reaction, *Cement Concr. Res.* 173 (2023) 107293.
- [65] A. Leemann, Z. Shi, J. Lindgård, Characterization of amorphous and crystalline ASR products formed in concrete aggregates, *Cement Concr. Res.* 137 (2020) 106190.
- [66] A. Leemann, L. Sanchez, Internal alkali transport in recycling concrete and its impact on alkali-silica reaction, *Cement Concr. Res.* 174 (2023) 107334.
- [67] W. Wang, T. Noguchi, I. Maruyama, Mechanism understanding of alkali-silica reaction in alkali-activated materials system, *Cement Concr. Res.* 156 (2022) 106768.
- [68] C.F. Dunant, K.L. Scrivener, Micro-mechanical modelling of alkali–silica-reaction-induced degradation using the AMIE framework, *Cement Concr. Res.* 40 (4) (2010) 517–525.
- [69] R.B. Figueira, R. Sousa, L. Coelho, M. Azenha, J.M. de Almeida, P.A.S. Jorge, C.J.R. Silva, Alkali-silica reaction in concrete: mechanisms, mitigation and test methods, *Constr. Build. Mater.* 222 (2019) 903–931.
- [70] H. Jin, S. Ghazizadeh, J.L. Provis, Thermodynamic modelling of alkali-silica reactions in blended cements, *Cement Concr. Res.* 181 (2024) 107543.
- [71] A. Gholizadeh Vayghan, F. Rajabipour, J.L. Rosenberger, Composition–rheology relationships in alkali–silica reaction gels and the impact on the gel's deleterious behavior, *Cement Concr. Res.* 83 (2016) 45–56.
- [72] P.J.M. Monteiro, K. Wang, G. Sposito, M.C.d. Santos, W.P. de Andrade, Influence of mineral admixtures on the alkali-aggregate reaction, *Cement Concr. Res.* 27 (12) (1997) 1899–1909.
- [73] S. Urhan, Alkali silica and pozzolanic reactions in concrete. Part 1: interpretation of published results and an hypothesis concerning the mechanism, *Cement Concr. Res.* 17 (1) (1987) 141–152.
- [74] Z. Shi, B. Ma, B. Lothenbach, Effect of Al on the formation and structure of alkali-silica reaction products, *Cement Concr. Res.* 140 (2021) 106311.
- [75] Z. Deng, Utilization of lithium nitrate to mitigate alkali–silica reaction of architectural glass mortar: characteristics and mechanisms, *Constr. Build. Mater.* 315 (2022) 125433.
- [76] S.M.H. Shafaatian, A. Akhavan, H. Maraghechi, F. Rajabipour, How does fly ash mitigate alkali–silica reaction (ASR) in accelerated mortar bar test (ASTM C1567)? *Cement Concr. Compos.* 37 (2013) 143–153.
- [77] Z. Shi, C. Shi, S. Wan, Z. Ou, Effect of alkali dosage on alkali-silica reaction in sodium hydroxide activated slag mortars, *Constr. Build. Mater.* 143 (2017) 16–23.